Adsorption and Activation of CO over Flat and Stepped Co Surfaces: A First Principles Analysis

Qingfeng Ge[†,‡] and Matthew Neurock*[,‡]

Department of Chemistry and Biochemistry, Southern Illinois University, Carbondale, Illinois 62901, and Department of Chemical Engineering, University of Virginia, Charlottesville, Virginia 22903

Received: January 23, 2006; In Final Form: April 18, 2006

The adsorption and activation of CO over flat Co{0001}, corrugated Co{11$\bar{2}$0}, and stepped Co{10$\bar{1}$2} and Co{11$\bar{2}$4} surfaces have been analyzed using periodic density functional theory calculations. CO strongly chemisorbs on all these surfaces but does not show a strong dependence on the surface structure. The calculated structure of adsorbed CO on Co{0001} at 1/3 monolayer (ML) of coverage was found to be in good agreement with the experiment. The barrier for CO dissociation over Co{0001} was found to decrease with decreasing CO coverage, taking on a value of 232 kJ/mol at 1/4 ML and 218 kJ/mol at 1/9 ML. The presence of the "zigzag" channel on Co{11$\bar{2}$0} enhances the reactivity slightly by reducing the barrier for CO dissociation to 195 kJ/mol. In contrast, the stepped Co{10$\bar{1}$2} and Co{11$\bar{2}$4} surfaces are much more active than the flat and corrugated surfaces. Both stepped surfaces provide direct channels for CO dissociation that do not have barriers with respect to gas-phase CO. In general the activation barriers lower as the reaction energies become more exothermic. Reconstruction of the step edges that occur in the product state, however, prevents a linear correlation between the reaction energy and the activation energy.

1. Introduction

The past decade has witnessed a strong resurgence of interest in Fischer−Tropsch (FT) synthesis as a process critical for the conversion of methane to liquid fuels and the clean processing of coal to chemicals and energy. Much of the interest has been motivated by the drive to remove the dependence on crude oil. Coal can be used as feedstocks in gasification processes and produce syngas (CO and H_2), the feed for FT synthesis. Syngas can also be produced via the partial oxidation or the steam-reforming of natural gas.[1] FT synthesis involves the conversion of syngas into higher aliphatic hydrocarbons that are subsequently used in the production of higher olefins, gasoline, diesel fuel, waxes, and oxygenates. FT synthesis is comprised of a complex network of elementary bond-breaking and bond-formation steps. These steps include CO and H_2 activation as well as hydrogenation and chain growth over supported metal catalysts. There is a delicate balance between bond-breaking and bond-formation steps that ultimately controls the catalytic activity and selectivity of this system. For example, transition metals to the left in the periodic table will readily activate CO, but the products from these activation steps, i.e., surface carbon and oxygen, are too strongly bound to the surface and thus hinder the subsequent hydrogenation and carbon coupling reactions. Transition metals to the right, on the other hand, are generally not active enough to dissociate CO.[2,3] The ideal metals for FT synthesis then are those that can promote CO activation yet provide a balanced degree of surface hydrogenation and C−C coupling in order to produce longer chain hydrocarbon products. Cobalt appears to have optimal properties thus allowing CO to dissociate and subsequently undergo both hydrogenation and coupling reactions with similar rates. Iron which is just to the left in the periodic table will more readily activate CO but has a strong tendency to form surface carbides. Iron dominated much of the earlier FT processes but has since been replaced by Co for processes based on the conversion of natural gas. Nickel which lies just to the right of Co is somewhat less active in dissociating CO than Co but undergoes more rapid hydrogenation thus leading to preferential formation of methane. Both Ru-promoted Co as well as base-promoted iron appear to be attractive alternatives.[4]

A significant number of studies[4−7] have examined the mechanism for FT synthesis and the optimal conditions to form the desired products since the initial discovery of this process by Fischer and Tropsch over 70 years ago. Many of these studies have focused on the preparation and characterization of different catalysts. These studies provided essential information for the design of industrial FT reactors and the catalysts that are currently used. It is generally agreed that both CO and H_2 adsorb and subsequently dissociate over the metal. These steps are followed by catalytic propagation steps which include the hydrogenation and coupling of the hydrocarbon intermediates to create longer chain hydrocarbons. The catalytic chain growth is ultimately terminated through either hydride elimination paths that lead to olefins or hydrogenation steps which lead to the formation of alkanes. The molecular transformations which control the mechanism and the kinetics in this system, and in addition, the influence of the atomic scale features of the supported metal catalysts on the catalytic activity, however, are not very well understood. A more detailed understanding of the elementary steps involved in the reaction and the influence of catalyst surface structure will help to provide a more detailed analysis of the mechanism, establish more reliable kinetic models, and aid in the development of structure−reactivity relationships.

* To whom correspondence may be addressed. E-mail: Neurock@virginia.edu.
† Southern Illinois University.
‡ University of Virginia.

10.1021/jp060477i CCC: $33.50
Published on Web 07/18/2006

The adsorption and dissociation of CO are the first steps in the mechanism and thought to be critical in controlling catalytic activity, as CO dissociation is believed to be the rate-limiting step.[8] As such, the adsorption of CO on cobalt surfaces has been widely examined. Most of these studies have focused on the {0001} surface of Co. Thermal desorption (TPD),[9,10] work function measurements,[10,11] low-energy electron diffraction (LEED),[9−13] and photoelectron spectroscopy[13,14] have all been applied to characterize CO adsorption on Co surfaces. CO was found to adsorb molecularly on Co{0001} for temperatures up to 450 K.[9,11] At coverage less than 1/3 of a monolayer (ML), adsorbed CO molecules form an ordered $(\sqrt{3} \times \sqrt{3})$R30° structure where CO adsorbs at the atop site with the carbon end of the molecule directed toward the surface and the C−O bond normal to the surface.[10−12] At the saturation coverage, seven CO molecules can be packed into a $(2\sqrt{3} \times 2\sqrt{3})$R30° structure thus forming an overlayer of CO with 0.58 ML coverage.

The adsorption of CO on Co{10$\bar{1}$0} has been examined in detail by King and co-workers.[15−17] On defect-free Co{10$\bar{1}$0}, the adsorption of CO was shown to be nondissociative. The binding sites of CO and the overlayer structures were found to vary with the CO coverage. Strong relaxation has been reported for both the clean Co{11$\bar{2}$0} [18] and{10$\bar{1}$2} surfaces.[19] Adsorption of CO on these surfaces has been shown to form a (3×1) structure, although the nature of the structures is different. The CO-induced (3×1) structure on Co{11$\bar{2}$0} was explained with a "missing row − added row" model by Venvik et al. on the basis of scanning tunneling microscopy studies.[20] In contrast, the (3×1) structure on the Co{10$\bar{1}$2} surface was attributed to a pure CO overlayer by the same authors.[21] On Co{11$\bar{2}$0}, Papp reported that the dissociation of CO takes place at ∼360 K,[14] while Bardi and Rovida found it to occur after heating to 420 K.[22] On the other hand, Geerling et al. reported that CO would desorb molecularly up to 470 K on the same surface.[23] On Co{10$\bar{1}$2}, dissociation of CO has been observed by heating the sample from 300 to 470 K.[19,24] While these studies have provided very useful fundamental information for CO adsorption and activation, it is clear that there are still a number of unanswered questions.

In the present paper, we present a density functional theory analysis of CO adsorption and dissociation over a number of Co surfaces. In particular, we examine the adsorption and activation of CO over the more open, corrugated {11$\bar{2}$0} surface, and the stepped {10$\bar{1}$2} and{11$\bar{2}$4} surfaces and compare the results with those for the ideal close-packed {0001} surface. The results show that while there is very little difference in the CO adsorption energy on these surfaces, the different environments on each of these surfaces significantly influence the calculated activation barriers.

2. Computation Details

The calculations described herein were carried out using a plane-wave density functional periodic slab method as implemented in the VASP code.[25−27] The electron−ion interactions were described by ultrasoft pseudopotentials[28] with a plane-wave cutoff energy of 320 eV. Increasing the cutoff energy up to 500 eV showed that the calculated adsorption energies and reaction barriers converged to within 10 kJ/mol. The chemisorption energies of CO and atomic O as well as the barrier for CO dissociation over Co{0001} in a (2×2) unit cell were provided in Table 1. The calculated C−O bond strength and bond distance of 1104.5 kJ/mol and 1.14 Å, respectively, at this cutoff energy agree well with those from experiements.[29]

TABLE 1: Chemisorption Energies of CO ($\Delta E_{ads,CO}$) and Atomic O ($\Delta E_{ads,O}$) and CO Dissociation Barrier (ΔE^*_{diss}) over Co{0001} as Well as Atomization Energy of CO at Different Plane Wave Cutoff Energies

		320 eV cutoff energy	400 eV cutoff energy	500 eV cutoff energy
$\Delta E_{ads,CO}$ (eV)	fcc	−1.6512	−1.6048	−1.6105
	hcp	−1.6652	−1.6184	−1.6209
$\Delta E_{ads,O}$ (eV)	fcc	−5.5565	−5.4312	−5.4183
	hcp	−5.6386	−5.5337	−5.5209
D_{CO} (eV)		11.4477	11.2723	11.2627
ΔE^*_{diss} (eV)		2.4135	2.4145	2.4390

TABLE 2: Bond Lengths, Adsorption Energies, and Stretching Frequencies for Chemisorbed CO on Co{0001} at Different Adsorption Sites at 1/3 ML

	atop	bridge	fcc	hcp
d_{C-O} (Å)	1.17	1.19	1.19	1.19
d_{C-Co} (Å)	1.76	1.91(2)	2.00(3)	1.98(3)
ν_{C-O} (cm^{-1})	1994	1819	1787	1757
$\Delta E_{ads,CO}$ (kJ/mol)	−156.2	−149.2	−154.8	−156.1

Spin polarization was found to be essential in order to appropriately account for the ferromagnetic nature of Co and the calculated adsorption energies and was therefore included in all the calculations. The Perdew-Wang form of generalized gradient corrections was used to calculate the exchange and correlation energies.[30] Supercells of varying cell sizes and number of metal layers were used in our calculations to model different surfaces. The details for each surface are provided in the following corresponding sections. The Monkhorst−Pack[31] mesh was used to sample the surface Brillouin zone and the density of *k*-points was kept at ∼0.05 $Å^{-1}$. Throughout our calculations, we used a one-sided slab approach, i.e., placing adsorbates on one side of the slab. The vacuum region between the neighboring slabs was specified to be over 10 Å. We have successfully applied the same approach with similar parameters to various different systems.[32−35] The adsorbate atoms as well as the Co atoms in the topmost layers of the slab were optimize according to the forces calculated quantum mechanically. Transition states were located by using the nudged elastic band (NEB) method and its improvements developed by Jonsson and co-workers.[36−38] Transition states isolated with NEB were further optimized by using a quasi-Newton algorithm in order to minimize the forces on each of the movable atoms. Normal mode harmonic frequencies were calculated for all the transition states and for selected adsorption geometries as implemented in the latest version of VASP.[39]

3. Results and Discussions

The adsorption of CO on the close-packed {0001} surface was examined first and the results were compared with the detailed experimental structures. This comparison served as a test for the model chosen and for the parameters used in our calculations. The calculations for CO adsorption at different sites on Co{0001} were performed using $(\sqrt{3} \times \sqrt{3})$R30° and (2×2) surface unit cells with a slab of four metal layers and a vacuum space of 14.3 Å, corresponding to 1/3 and 1/4 ML CO coverage, respectively. The adsorption energies ($\Delta E_{ads,CO}$) and structural parameters as well as the C−O stretching frequencies for chemisorbed CO at various high-symmetry sites for the $(\sqrt{3} \times \sqrt{3})$R30° structure are summarized in Table 2. In the results presented here and what follows, the adsorption energy is calculated as the total energy difference between the adsorbate(s) − slab and the sum of adsorbate(s) and slab calculated separately. The negative value of the adsorption energy indicates

that the adsorption is an exothermic process. The calculated C−O and C−Co bond distances (d_{C-O} and d_{C-Co}) for CO adsorption on the atop site are in good agreement with that from the LEED analysis.[12] The calculated adsorption energies as well as the vibrational frequencies are in general agreement with those from TPD and infrared experiments.[23,40] At 1/3 ML, CO adsorbs most favorably on atop sites with an adsorption energy of −156.2 kJ/mol. This is not significantly more stable than that for CO at the hexagonal-close-packed (hcp) sites. As the coverage is decreased to 1/4 ML, the chemisorption bond is strengthened by ∼2 kJ/mol and adsorption at the hcp sites becomes slightly more favorable. However, we note that both the changes in the CO adsorption energy with coverage and the differences of the adsorption energy between different adsorption sites are on a similar order to the convergence and within the uncertainty level of the current theory.[41−43] Ultimately, the entropic contribution to the total free energy may determine which site will be populated at elevated temperatures under experimental conditions.

3.1. Coverage Effect on CO Dissociation. The surface coverage of the adsorbate has a strong effect on C−O bond activation. Chemisorbed CO forms a $(\sqrt{3} \times \sqrt{3})R30°$ overlayer on Co{0001}. Its dissociation to form coadsorbed C and O adatoms in the same unit cell is strongly endothermic, with an overall reaction energy of 220 kJ/mol with respect to the chemisorbed CO. The reaction barrier would be even higher, thus CO will not dissociate but instead desorb at this surface coverage. The lack of CO dissociation was also observed experimentally at this coverage.[10−12] The large overall reaction endothermicity is largely the result of sharing of the strongly bound C and O adatoms that form as the result of reaction. The reaction energy indeed decreases from 220 kJ/mol down to 92.1 kJ/mol if the C and O adatoms that result from the dissociation occupy the most stable hcp hollow sites and form their own $(\sqrt{3} \times \sqrt{3})R30°$ overlayer. The differences are attributed to the lower coverages that result from separating the C and O adatoms. The overall surface coverage in the product state is reduced from 2/3 ML to 1/3 ML. The decrease in the surface coverage reduces the repulsive interactions between C and O adatoms significantly. The reaction now becomes 64.2 kJ/mol exothermic with respect to the gas-phase CO.

The dissociation was subsequently examined in a (2 × 2) surface unit cell, corresponding to a CO coverage of 1/4 ML. At this coverage, the adsorption energies of chemisorbed CO at different sites was found to be similar to that on the $(\sqrt{3} \times \sqrt{3})R30°$: −160.0 kJ/mol at atop site, −159.3 kJ/mol in face centered cubic (fcc), and −160.4 kJ/mol in hexagonal close packed (hcp) site, respectively. The C and O adatoms that form both favor the hcp sites in separate (2 × 2) structures. With respect to hcp-adsorbed CO, the overall reaction energy to form C and O adatoms in separate (2 × 2) structures was found to be 60.1 kJ/mol. If the C and O adatoms that form remain in the same (2 × 2) unit cell whereby the C adatom sits in an hcp site and the O atom in an fcc site (the most favorable structure), the overall reaction energy becomes 65 kJ/mol higher in energy than that where the C and O adatoms occupied separate (2 × 2) unit cells. The hcp C and fcc O combination was found to be ∼26 kJ/mol more stable than if coadsorbed C and O adatoms occupy hcp sites. These energy differences indicate that there is a strong repulsive interaction between coadsorbed C and O adatoms.

Two different reaction pathways were found for the dissociation of CO on the closed packed Co{0001} surface by examining the symmetry of the surface, as shown in the upper panel of Figure 1:[44] In path I, CO dissociates into neighboring equivalent hollow sites resulting in a transition state which occupies two adjacent bridge sites of the close-packed Co atoms. In path II, CO dissociates over the top of a surface Co atom. The final state for path II corresponds to one in which the C and O adatoms occupy nonequivalent hollow sites on the opposite sides of the surface Co atom. These same sites can also be reached by the diffusion of the C and O adatoms in the product state of path I. The overall reaction energies for paths I and II are 150.5 and 124.8 kJ/mol, respectively. The structure of the calculated transition state for path I is shown in the lower panel of Figure 1. In this transition state, the C adatom is displaced slightly from the 3-fold hcp site with three C−Co bonds at 1.773, 1.836, and 1.990 Å, respectively. The O adatom product that results begins to form three bonds with the surface Co atoms with distances at 1.923, 1.923, and 2.203 Å, respectively. The C−O bond distance at the transition state is 1.807 Å, which is significantly longer than the C−O bond length in molecular CO. The highly stretched C−O distance at the transition state is in accord with the fact that CO dissociation involves a late transition state and with the previous reports for CO dissociation on Co and on other metals.[44−47] Normal-mode frequency analysis showed that this configuration has only one imaginary mode corresponding to C−O stretch, thereby confirming that this is a transition state for CO dissociation. The corresponding activation barrier at this transition state is 232.9 kJ/mol. The activation barrier for path II was shown to be higher than that for path I on Pt{111} and Ni{111}. It was also true for CO dissociation on Co{0001}. We therefore did not explore path II very extensively. We noticed that metal sharing at both the transition and final state exists for CO dissociation at this coverage which will lead to higher activation barriers. In fact, the distance between the neighboring O and C adatoms is only ∼2.5 Å, i.e., one lattice spacing, in the final state for path I while the C−O distance at the transition state is ∼1.81 Å. Our

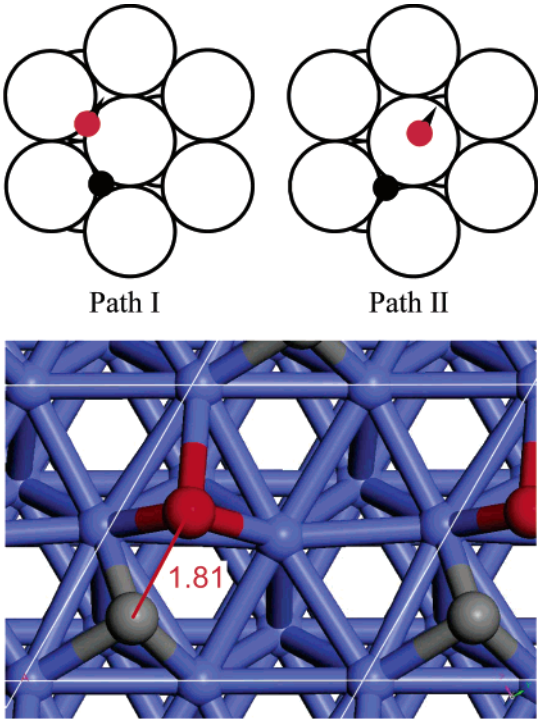

Figure 1. (upper panel) Schematic top views of two possible activation pathways to dissociate C−O bond on a close-packed surface (adapted from ref 44). (lower panel) Transition state structure of CO dissociation on Co{0001} in a (2 × 2) surface unit cell.

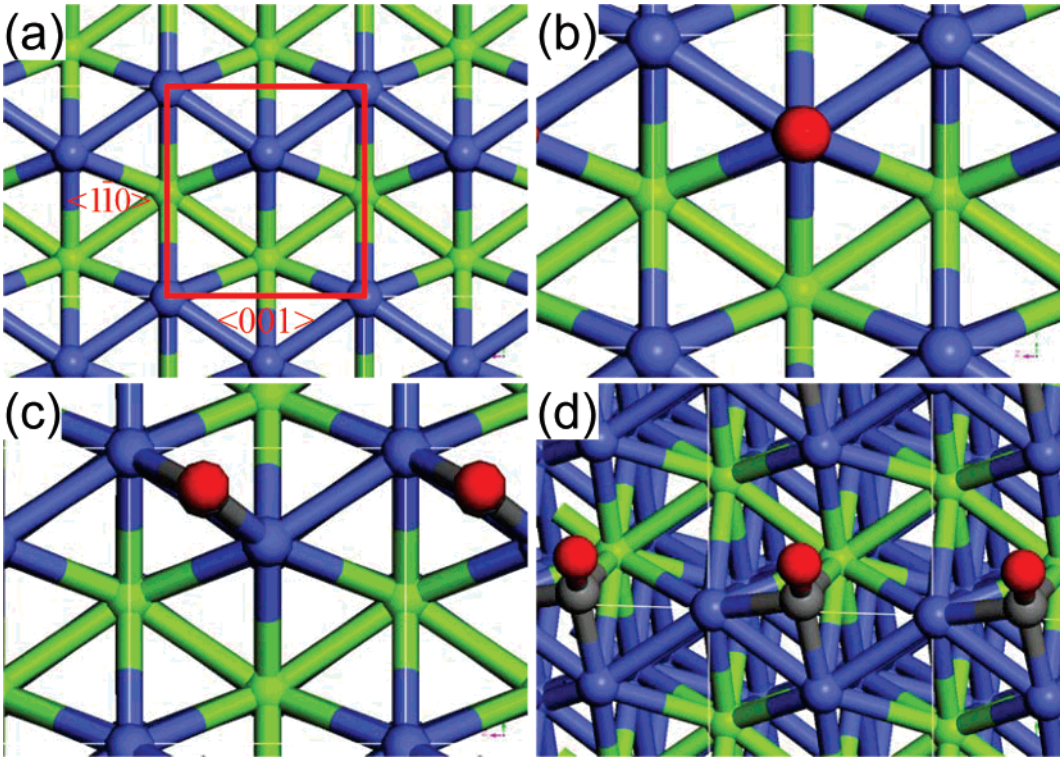

Figure 2. Top view of the Co{11$\bar{2}$0} surface (a) and CO (red and gray spheres) adsorption at three different sites, (b), (c), and (d), on Co{11$\bar{2}$0}. The surface consists of zigzag rows of atoms separated by a trench. The surface ridge atoms are in blue and the subsurface trench atoms are in green. The top view of CO bound to (b) atop site and (c) a bridge site. (d) is a tilt image of CO in the hollow site consisting of two ridge atoms and one trench atom. See Table 3 for detailed structural parameters.

results showed that this small separation between the two strongly chemisorbed adatoms would induce strong repulsive interactions between the adatoms, by ~65 kJ/mol as compared with C and O adatoms calculated in separate (2 × 2) unit cells. This strong repulsive interaction between C and O in the final state increases the total energy of the products which leads to a highly endothermic system and a very high activation barrier for CO dissociation.

The effect of the repulsive interactions on the reaction barrier can be illustrated by performing calculations at even lower initial surface coverages of CO. In the present study, the low coverage system was modeled by using a (3 × 3) surface unit cell, corresponding to an initial CO coverage of 1/9 ML. The overall reaction becomes less endothermic than that in the ($\sqrt{3} \times \sqrt{3}$)-R30° and (2 × 2) systems. The energy difference between the initial and final states along path I decreases from 150.5 kJ/mol at 1/4 ML to 76.5 kJ/mol at 1/9 ML. This value is close to the overall reaction energy calculated separately for C and O adatoms in a (2 × 2) unit cell. The decrease in the overall reaction energy is due to the lowered repulsive interactions between coadsorbed C and O adatoms at the low coverage. In this case the combined coverage for C and O adatoms is 2/9 ML. The transition state determined for the (2 × 2) surface unit cell was reoptimized for the (3 × 3) surface unit cell. The structure of the relaxed transition state is very similar to that found in the (2 × 2) calculation. The C−O distance at the transition state is 1.813 Å, which is only slightly longer than that in the (2 × 2) unit cell. The activation barrier for CO dissociation is decreased from 232 kJ/mol at 1/4 ML to 218 kJ/mol at 1/9 ML. We note that the decrease in activation is not as significant as the change in the overall reaction energy. This can be attributed to the fact that C and O adatoms still share a common surface Co atom at the transition state. The high barriers for CO dissociation even at low coverages are consistent with the experimental observations that the dissociation does not occur on the {0001} surface at temperatures as high as 450 K.[23]

3.2. Effect of Steps on CO Dissociation. It has been demonstrated both experimentally and theoretically that defect sites lead to lower metal coordination numbers and thus result in stronger adsorbate binding to the metal and enhanced adsorption energies.[48,49] These high binding energy sites may significantly improve the catalytic reactivity for reactions that are controlled by bond-breaking processes and may play an important role in the activation of CO. In the present study, the{11$\bar{2}$0}, {10$\bar{1}$2}, and {11$\bar{2}$4} surfaces of Co, were constructed in order to examine the effect of defect sites on CO dissociation. The {11$\bar{2}$0} surface is more open and corrugated than the close-packed {0001} surface although it is not considered to be a stepped surface. On the other hand, both {10$\bar{1}$2} and {11$\bar{2}$4} contain steps with the latter having double steps as well as kinks within a single unit cell. We have explored the effect of these defects on CO adsorption and C−O bond activation and will present the results in turn for each surface in the remainder of the section.

3.2.1. Co{11$\bar{2}$0}. We first examined CO, C, and O adsorption on the {11$\bar{2}$0} surface. The {11$\bar{2}$0} surface is corrugated and consists of zigzag rows of surface "ridge" Co atoms separated by a "trench". The slab used to simulate the surface consists of five Co layers and a vacuum region of 14.6 Å. The Co atoms in the top three layers as well as the adsorbate atoms were all allowed to relax during geometry optimization. The structural characteristics of this surface are shown in Figure 2a, with the ridge and trench Co atoms being colored differently for clarity. The surface unit cell used in the calculations of CO, C, and O adsorption is also labeled in Figure 2a. The adsorption of CO on different sites across the surface, shown in parts b, c, and d of Figure 2, was calculated. The adsorption energy as well as

TABLE 3: Bond Distances and Adsorption Energies of Chemisorbed CO on Co{1120} at Different Adsorption Sites at 1/2 ML

	atop	bridge	hollow
d_{C-O} (Å)	1.17	1.18	1.23
d_{C-Co} (Å)	1.76	1.90, 1.92	1.93, 2.00, 2.04
$\Delta E_{ads,CO}$ (kJ/mol)	−158.7	−159.6	−159.0

C−O and C−Co distances are listed in Table 3. The adsorption energies for all the sites examined here are similar, with a variation of only ∼1 kJ/mol. CO adsorption on the bridge site, with an adsorption energy of −159.6 kJ/mol, is only slightly more stable than that on the atop and hollow sites. Unlike the {0001} surface, two of the three hollow site Co atoms are in the surface plane whereas the third resides in the subsurface layer. Two stable adsorption configurations for C and O adatoms in Figure 3 were determined. In parts a and c of Figure 3, the carbon and oxygen adatoms occupy the long-bridge sites that are formed by two ridge Co atoms across the trench. In these sites, the adatoms are in highly symmetric positions and interact directly with the two surface ridge atoms and two subsurface trench atoms. The distances of C adatom to the two ridge Co atoms are 1.82 Å and to the two trench atoms are 1.90 Å. The O−Co distances in a similar configuration (Figure 3c) are 1.90 and 2.05 Å, respectively, and longer than the corresponding C−Co distances. On the other hand, carbon and oxygen adatoms in the sites shown in parts d and d of Figure 3 interact directly with three surface ridge Co atoms in the same row and one subsurface trench atom. Oxygen contains excess lone pairs of electrons which act to increase Pauli repulsion; this can lead to longer O−Co distances and higher heights of oxygen above the Co surface. The binding energies for C in these two adsorption configurations are very similar: −684.4 and −678.3 kJ/mol, respectively. The difference in binding energy for oxygen adatoms in the two configurations is slightly greater: −524.5 and −533.5 kJ/mol, respectively. Note that the relative stability of O adatoms in these two sites is reversed from that of C adatoms. On the basis of the adsorption energies of C, O, and CO at the most stable sites, the overall reaction for CO dissociation on Co{11$\bar{2}$0} is calculated to be exothermic with respect to gas-phase CO by −104.4 kJ/mol *but* still endothermic with respect to chemisorbed CO, by 55.2 kJ/mol.

The dissociation pathways for chemisorbed CO were studied in a unit cell that is twice that of the surface unit cell shown in Figure 2a in both surface directions. The resulting cell has four times as many Co atoms than the cell used in the calculations for C, O, and CO adsorption shown above. Consequently, if we examine only one CO molecule within the cell, the coverage of CO is reduced to 1/8 ML. The transition state for CO dissociation was also determined on this surface. Figure 4 shows the initial reactant state, the transition state, and the final product state along the reaction pathway. CO adsorbs at the hollow site and subsequently dissociates into the state where C and O adatoms occupy the "zig" sites across the trench. The overall reaction energy for this path is endothermic by 58.4 kJ/mol, which is only 3.2 kJ/mol higher than the value calculated with the adsorption energies of C and O adatoms from separate calculations with coverages at 1/8 ML, respectively. At the transition state, shown in Figure 4b, the C−O distance is stretched to ∼2.2 Å. The activation barrier corresponding to this transition state is 195 kJ/mol. Normal-mode analysis has shown that only the mode corresponding to the C−O stretching is imaginary, thereby confirming that this configuration is a transition state for CO dissociation.

3.2.2. Co{10$\bar{1}$212}. The adsorption of CO, C, and O species was calculated next on the {10$\bar{1}$2} surface. The slab to simulate the surface has nine layers, which is equivalent to three close-packed layers, and a vacuum region of 14.2 Å. The side view of the surface in Figure 5a clearly shows the steps on the surface. If the surface is viewed along the ⟨010⟩ direction, the surface consists of a channel separated by a ridge of two uneven rows of surface Co atoms. After relaxation, the height difference between the two rows is reduced from 0.50 Å for bulk termination to 0.43 Å. On the other hand, when the surface is viewed based on the close-packed {0001} plane, the step consists of two features: a close-packed facet followed by a rectangle facet. The {0001} terrace consists of only one close-packed Co atomic row. The angles between different facets after surface relaxation are also shown in Figure 5a. The two sides of the rectangular facet are 2.537 and 2.438 Å, making it close to a square. The top and perspective views of the surface together with the (2 × 1) surface unit cell used in our calculations are shown in parts b and c of Figure 5.

A series of different sites for CO adsorption were examined. The calculated adsorption energies and structural parameters are summarized in Table 4. In addition to the bond distances and adsorption energy of chemisorbed CO at different sites, we also included the tilt angle of CO away from the surface normal in the table. These adsorption sites can be categorized in four groups: atop sites (A, C), bridge sites (B, F, and G), 3-fold hollow sites (H, I), and bridging sites (D, E). The two atop sites examined, A and C, have similar adsorption energies for CO: −154.7 and −158.1 kJ/mol, respectively. The C−O molecular axis for CO adsorbed in the atop sites is almost aligned with the surface normal direction. The adsorption energies for three bridge sites are −164.6, −161.0, and −151.3 kJ/mol, with the bridge site formed by the shorter side of the rectangle (B) being the most stable. This uneven bridge site is the most stable adsorption site for CO among all the sites examined on Co-{10$\bar{1}$2}. Bridge site G, which is on the lower side of the rectangle and below the surface plane, has the smallest adsorption energy for CO among all the bridge sites. In Table 3, we also listed CO adsorption on one additional bridge site, site F1. In site F1, the C atom of the CO molecule bridges the same surface Co atoms as in site F. However, the CO molecule has a different tilt angle. With the current convergence criteria, CO adsorption in site F1 was also found to be a minimum with an adsorption energy of −158.1 kJ/mol. The adsorption of CO at the two 3-fold hollow sites, H and I, also has similar adsorption energies: −151.7 and −149.0 kJ/mol, respectively. Due to the location of these hollow sites, the molecular axis of CO tilts toward opposite directions along ⟨21$\bar{1}$⟩. Two unique 4-fold bridging adsorption configurations were formed on the Co-{10$\bar{1}$2} surface upon CO adsorption. In these two configurations, shown in Figure 6, there are not only four C−Co bonds formed but also one O−Co bond. In these sites, the C−O bond is significantly stretched. Despite the numerous CO−surface bonds formed in these configurations, the strength of the CO−surface interaction is not stronger than many of the other configurations listed in Table 4. This is because the strength of the chemisorption bond is determined by the balance between the CO−surface bonds and surface relaxation/reconstruction and is related to the total energy of the adsorbate system.[50] On the other hand, the bond lengths of C−O and C−Co as well as C−O stretching frequency are influenced by the local bonding characteristics, which in turn is influenced by the charge mixing and transfer in forming the chemisorption bonds.

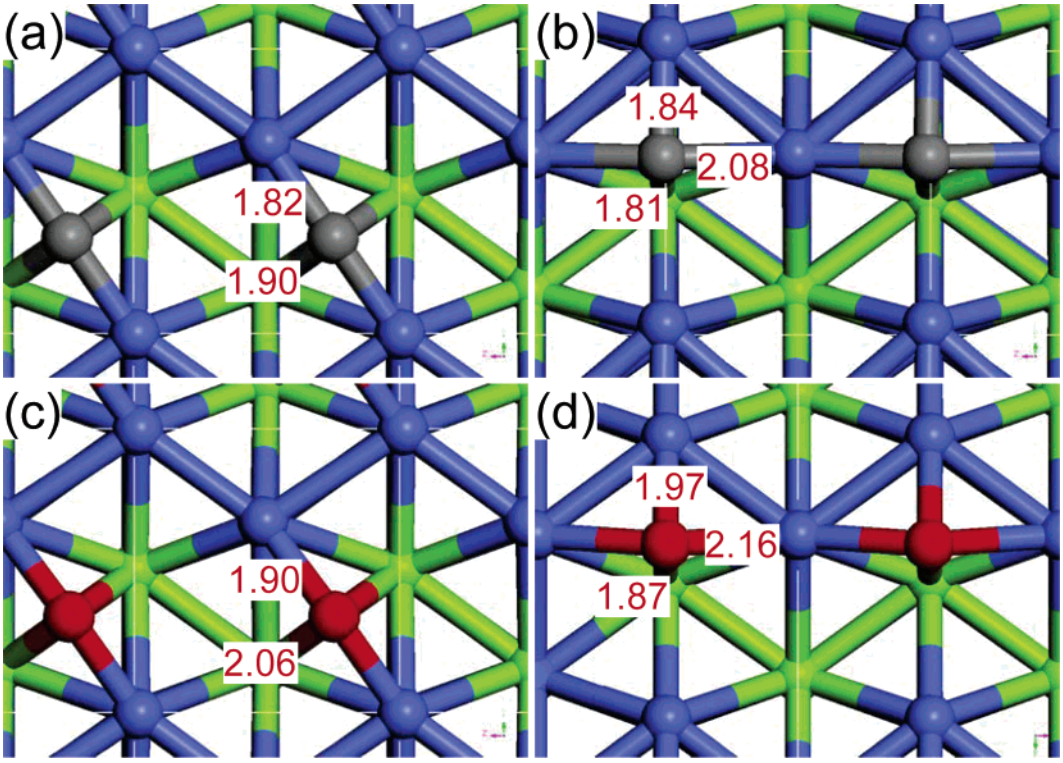

Figure 3. Top views of C (gray) and O (red) adatoms at different sites on Co{11$\bar{2}$0} at 0.5 ML. (a) and (b) are for carbon, and (c) and (d) are for oxygen. Blue and green spheres are for surface (ridge) and subsurface (trench) Co atoms. The C−Co and O−Co distances are also labeled.

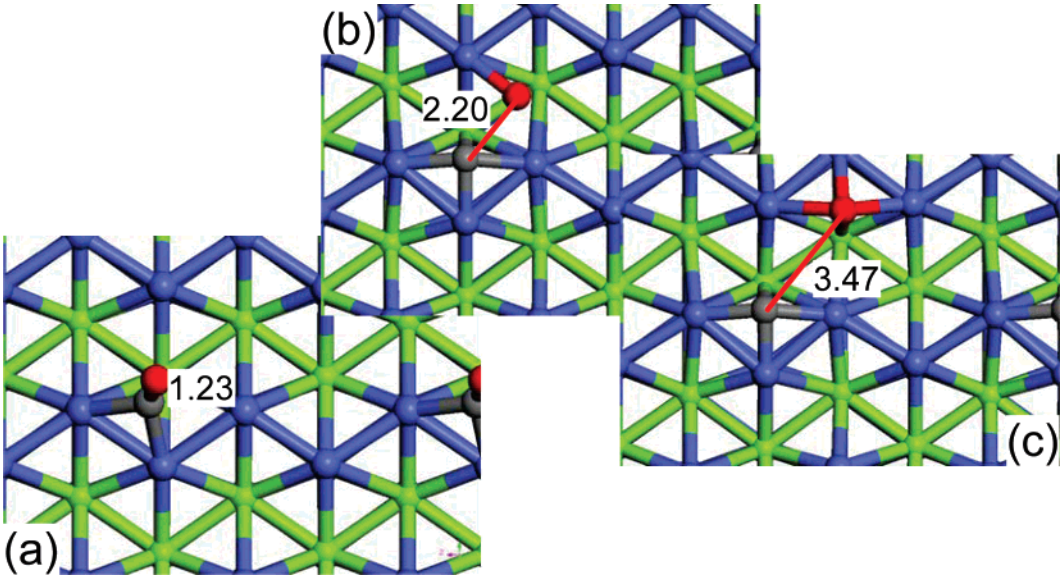

Figure 4. Schematic dissociation path for CO on Co{11$\bar{2}$0}: (a) initial state of chemisorbed CO; (b) transition state; (c) final state of coadsorbed C and O adatoms. The evolution of C−O distance along this reaction path is also shown.

Seven different starting configurations were examined to find the optimal binding sites for the carbon adatom on the Co{10$\bar{1}$2} surface. The results which are shown in Figure 7 indicate that there were only three stable adsorption sites, two in which the carbon was found at the 4-fold hollow sites and one in which carbon resides on a bridging Co site. A similar perspective view of the relaxed clean surface was also shown in Figure 7 for comparison. The most stable adsorption site is the original pseudo-4-fold hollow site on the step, as shown in Figure 7a. The adsorption energy for a C adatom at this site is −753.8 kJ/mol. Significant surface reconstruction was induced by C adsorption. The adsorption of the C adatom at the hollow site pushes the Co rows in ⟨010⟩ direction apart from 2.44 Å of the clean surface to 2.64 Å. The C adatom also interacts with the Co atom in the center of the hollow site directly underneath the C adatom. The four C−Co surface bonds are 1.90 Å whereas the C bond to the Co atom at the bottom of the ridge is 2.06 Å. Another stable 4-fold adsorption site is formed from the adsorption or binding of atomic C near site B shown Figure 7d. The adsorption brings rows of Co atoms across the channel together, resulting in the 4-fold-hollow-site-like configuration shown in Figure 7b. The adsorption energy of the C adatom at this site is −686.5 kJ/mol, significantly less than the original 4-fold site. The surface reconstruction upon C adsorption is stronger than that in Figure 7a and clearly visible in Figure 7b. The strong binding of the carbon adatom with the surface Co

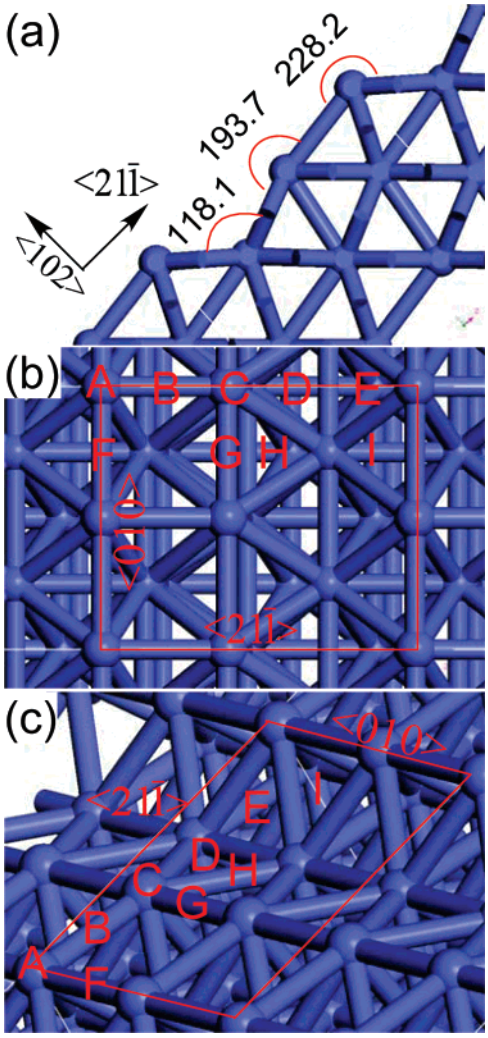

Figure 5. (a) Side, (b) top, and (c) perspective views of the Co{10$\bar{1}$2} surface. The directions ⟨102⟩ and ⟨21$\bar{1}$⟩ labeled in (a) correspond to normal and parallel directions to the surface plane. The angles that are labeled are reported in degrees. The vectors of the surface plane and the surface unit cell as well as the CO adsorption sites are also labeled in the top and perspective views.

TABLE 4: DFT Calculated Adsorption Energies and Structural Parameters of Chemisorbed CO on Co{10$\bar{1}$2} at Different Adsorption Sites

	ΔE_{ads} (kJ/mol)	d_{C-O} (Å)	d_{C-Co} (Å)	d_{O-Co} (Å)	θ (deg)
A	−158.1	1.166	1.770		−2.5
B	−164.6	1.185	1.861, 1.992		13.3
C	−154.7	1.169	1.769		1.5
D	−141.9	1.239	1.851, 2.035, 2.108, 2.151	2.160	−35.7
E	−149.2	1.247	1.838, 2.097, 2.057, 2.124	2.094	25.3
F	−161.0	1.182	1.899, 1.957		3.6
F1	−158.1	1.183	1.887, 1.948		−13.2
G	−151.4	1.190	1.920, 1.923		4.4
H	−151.7	1.219	1.898, 1.982, 1.990		−32.7
I	−149.0	1.211	1.952, 1.955, 2.025		17.5

atoms pulls the rows of the Co atoms across the channel from 3.64 Å (see Figure 7d) of the clean surface to 2.93 Å on the C-covered surface. The C adatom also interacts with the Co atom at the bottom of the channel. The four C−Co bonds are longer than the same bonds in the original 4-fold site, at 1.97 Å, and one shorter, at 1.89 Å. The strong C−Co interaction is counteracted by the reconstruction of the surface atoms, which results in a less strongly bonded state than in the site shown in Figure 7a. Carbon adsorption in the bridging site across the channel is also stable, with an adsorption energy of −699.0 kJ/mol. In this site, C forms two bonds to the Co atoms on the opposite side of the channel at 1.81 and 1.84 Å and two equal bonds to the Co atoms at the bottom of the channel at 1.91 Å.

The binding of the oxygen adatom was also examined on the Co{10$\bar{1}$2} surface. For an oxygen adatom, starting from the bridge site of the rectangle leads to an almost identical final configuration as that from the pseudo-4-fold site, as shown in Figure 8a. The adsorption energy of the O adatom in this site is −576.9 kJ/mol. Unlike the case for C adsorption, the binding of the O adatom leads to small changes in the Co surface structure, as shown in Figure 8a. The distances from C to the two Co atoms in the upper edge are 1.96 Å and to the two Co atoms in the lower edge 2.04 Å. Furthermore, oxygen adsorption in the vicinity of site B resulted in two metastable 3-fold sites: one on the terrace and another on the step, as shown in parts b and c of Figure 8. The adsorption energies of O adatoms at the two sites were calculated to be −520.2 and −541.0 kJ/mol, respectively. The binding of oxygen with the surface is not strong enough, however, to transform these 3-fold sites into the 4-fold-like site as that in the case of C adsorption. This may be prevented by the much greater Pauli repulsion for oxygen at these sites than for carbon. The bond distances for O to the edge Co atoms are shorter than those to the bottom of the channel. The bridging site was found to be stable for oxygen adatoms. The adsorption energy of oxygen in this configuration is −525.0 kJ/mol. Similar to C, O forms two bonds to the Co atoms on the opposite side of the channel at 1.89 and 1.91 Å and two equal bonds to the Co atoms at the bottom of the channel at 2.02 Å in this site.

On the basis of the calculated adsorption energies of C, O, and CO at the most stable adsorption sites, the overall reaction for CO dissociation on Co{10$\bar{1}$2} with respect to chemisorbed CO is exothermic by −61.5 kJ/mol. It is even more exothermic if it is calculated with respect to gas-phase CO, resulting in an overall reaction energy of −226.2 kJ/mol. Clearly, the energy landscape is significantly modified by the presence of the steps on the surface.

We further explored the reaction paths for CO dissociation and searched for transition states along these paths on Co{10$\bar{1}$2}. The two transition state structures shown in parts a and b of Figure 9 were isolated from different starting CO adsorption geometries. Figure 9a is the transition state found for CO initially adsorbed at site D in Figure 6a. In this transition state, the C adatom is in a distorted 4-fold bridging site and the O starts to form a bond with the neighboring Co atoms. The transition state has an activation barrier of 160.9 kJ/mol with respect to the initial CO adsorption state and is 18.9 kJ/mol higher than the gas-phase CO. The C−O bond is further stretched to 1.916 Å at this transition state as compared with that in the transition state on the close-packed {0001} surface. The second dissociation pathway proceeds with CO adsorbed in site H. The resulting transition state structure is illustrated in Figure 9b. In this transition state, the C atom bonds to the 3-fold site on the close-packed terrace and the O atom bridges the Co atoms of the longer side of the rectangle. The C−O bond is further stretched to 2.128 Å in this state. The corresponding activation barrier at this transition state is 123.0 kJ/mol with respect to the initially chemisorbed CO. More importantly, this transition state lies 28.7 kJ/mol below gas-phase CO, which will make CO dissociation spontaneous on the Co{10$\bar{1}$2} surface if dissociation proceeds at low coverages from the gas phase.

3.2.3. Co{11$\bar{2}$4}. The unit cell for the Co{11$\bar{2}$4} surface includes double steps and a kink, i.e., "zigzag" rows of Co atoms

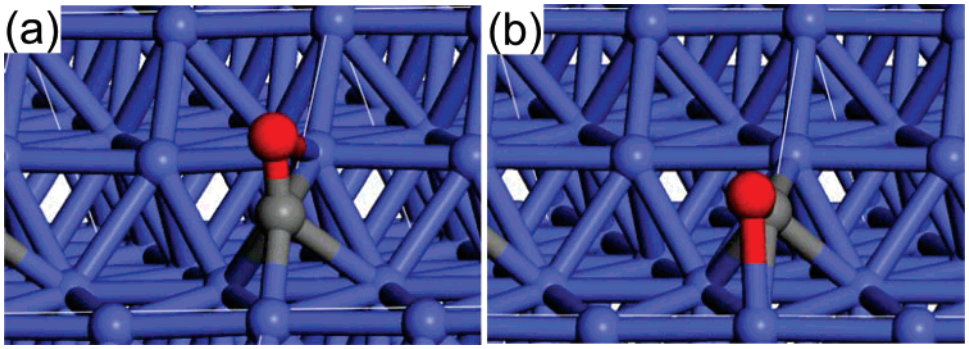

Figure 6. Perspective views of CO adsorption in the channel of the Co{10$\bar{1}$2} surface: (a) 4-fold bridging site D; (b) 4-fold bridging site E.

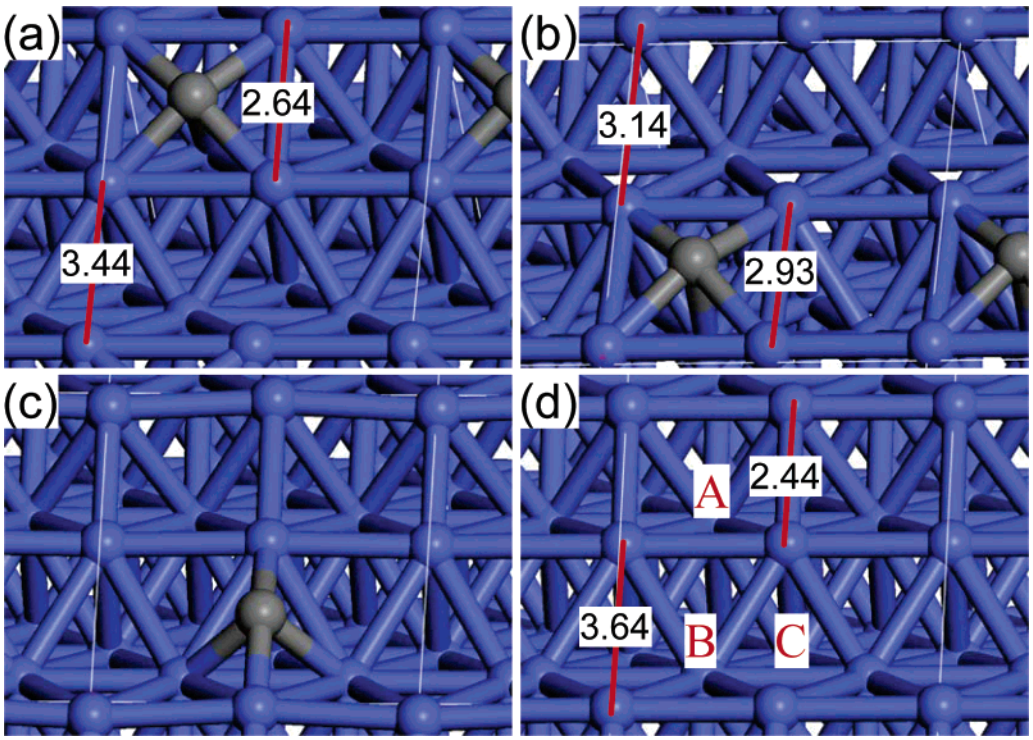

Figure 7. Perspective view of C adsorption on the Co{10$\bar{1}$2} surface: (a) the original pseudo-4-fold site; (b) the reconstructed pseudo-4-fold site in the channel; (c) bridging site across the channel; (d) relaxed surface for reference. See text for details.

separated by a "zagzig" row. The side and perspective views of the surface together with the surface unit cell used in our calculations along with the sites examined for CO adsorption are shown in Figure 10. The slab consists of seven layers of Co, equivalent to three close-packed layers, and a vacuum space of 11.5 Å. The relaxation of adsorbed CO at four different sites, A, B, C, and D, resulted to stable adsorption configurations, with adsorption energies of −150.1, −164.4, −141.7, and −141.1 kJ/mol, respectively. The C−O and C−Co bond distances in site A, an atop site, are 1.165 and 1.778 Å, respectively. In the bridging B site, the most stable site identified on this surface, the C−O bond length is 1.189 Å and C−Co bond distances are 1.870 and 1.957 Å. The adsorption in the higher coordination sites is less stable. The 3-fold-like site C at the bottom of step has an adsorption energy of −141.7 kJ/mol with a C−O bond length of 1.265 Å. In this site, the oxygen atom of the CO molecule also forms a bond with the Co atom in the upper step. The distances of the three C−Co bonds are 1.912, 1.907 and 2.058 Å and the O−Co distance is 2.131 Å. In site D, the carbon atom bonds to four Co atoms in the 4-fold site on the steps while the oxygen atom is bound to a Co atom in the upper step. The distances of the four C−Co bonds are in the range of 1.98−2.08 Å whereas the O−Co distance is 2.08 Å. The C−O bond is stretched to 1.291 Å at this site.

The adsorption of the C and O adatoms on the Co{11$\bar{2}$4} surface was also studied. A number of different starting geometries for these atomic species were examined, and the results shown in Figures11 and 12 are the stable configurations obtained after relaxation. For C adatom, adsorption in the 4-fold site (Figure 11a) was found to be more stable, with an adsorption energy of −717.0 kJ/mol. The C adatom at this site also interacts directly with a fifth Co atom in the next layer with a bond length of 2.194 Å. The average bond length for the other four C−Co bonds is 1.88 Å. The carbon adatom adsorbed in the configuration of Figure 11b is almost as stable, with an adsorption energy of −716.6 kJ/mol. This site is similar to the 4-fold bridging site on Co{10$\bar{1}$2} although the kink makes the local structure different on Co{11$\bar{2}$4}. This C adatom has three C−Co distances in the range of 1.83−1.85 Å and one at 1.944 Å. For oxygen adatoms, this site forms a 3-fold instead of 4-fold bridging site, as shown in Figure 12b. The adsorption of oxygen in the 4-fold hollow site (Figure 12a) is significantly less stable than that in the 3-fold site (Figure 12b). This is in direct contrast to the C adatom adsorption. The adsorption energies of oxygen

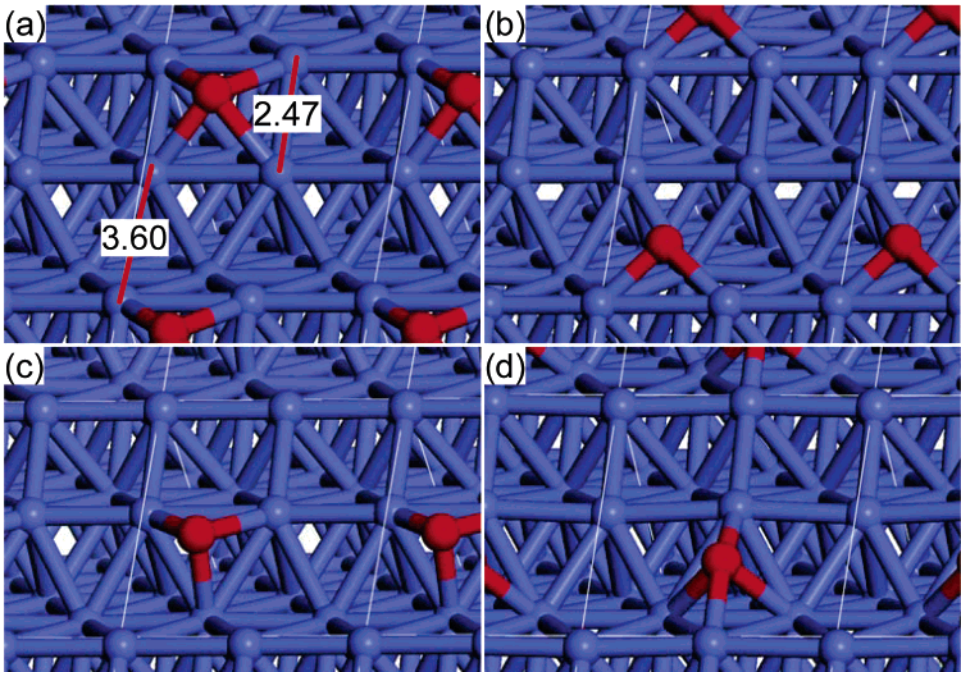

Figure 8. Perspective view of O adsorption on the Co{10$\bar{1}$2} surface: (a) pseudo-4-fold site; (b) 3-fold side on the terrace; (c) 3-fold site on the step; (d) bridging site across the channel.

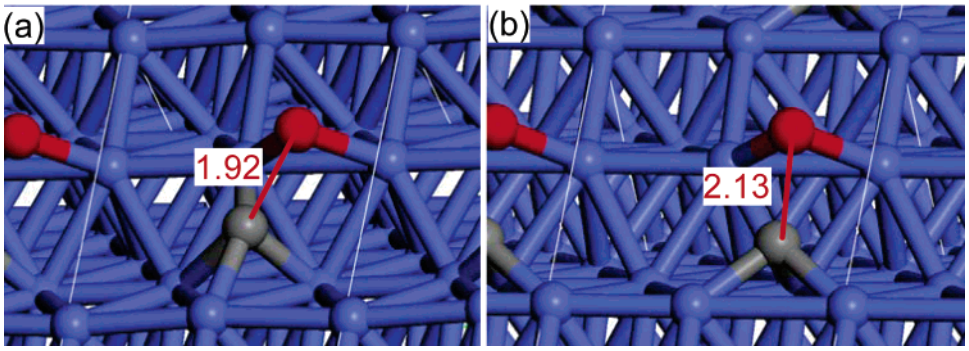

Figure 9. Transition states for CO dissociation across the steps of the Co{10$\bar{1}$2} surface with initial CO in different sites: (a) 4-fold bridging site−bridge site; (b) 3-fold site−bridge site.

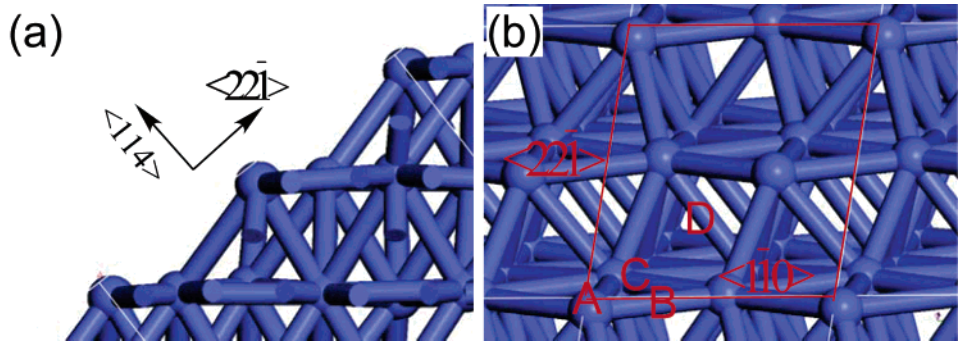

Figure 10. (a) Side and (b) perspective views of the Co{11$\bar{2}$4} surface. The directions ⟨114⟩ and ⟨22$\bar{1}$⟩ labeled in (a) correspond to normal and parallel directions to the surface plane. The vectors of the surface plane and the surface unit cell as well as the CO adsorption sites are also labeled in the perspective view.

in the 4-fold and 3-fold sites are −507.7 and −558.9 kJ/mol, respectively. In fact the adsorption energy of oxygen in the 4-fold site is similar to that of the remaining two 3-fold sites in parts c and d of Figure 12. The oxygen adsorption energies in parts c and d of Figure 12 are −503.4 and −500.0 kJ/mol, respectively. The dissociative adsorption of CO into a combination of C and O adatoms was energetically more favorable than the molecular chemisorption of CO in its most stable configuration by 7 kJ/mol. Therefore, the dissociation of chemisorbed CO on Co{11$\bar{2}$4} is exothermic, and the overall reaction energy as calculated with the most stable configurations of the adsorbates is −7 kJ/mol. The reaction energy for CO dissociation is −171.0 kJ/mol with respect to the gas-phase CO.

The reaction pathways for CO dissociation were explored and the transition states along different pathways on Co{11$\bar{2}$4} were determined. Transition state calculations were carried out for both the (1 × 1) and (2 × 1) surface unit cells. The results indicate that the transition state structures are similar and that

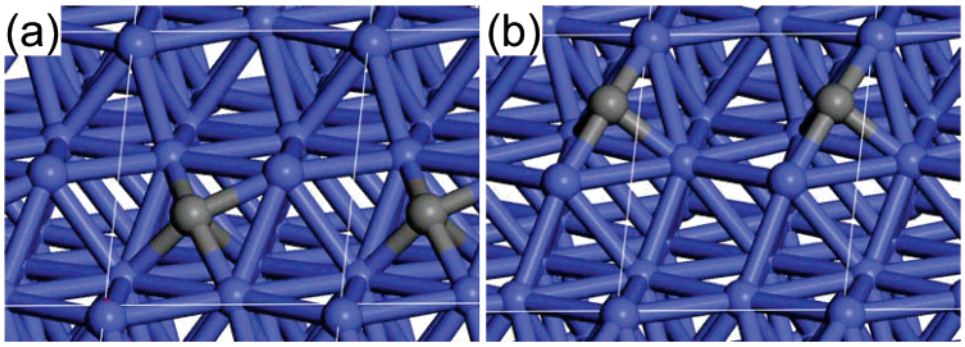

Figure 11. Perspective views of C adatoms adsorbed in two different sites on the Co{11$\bar{2}$4} surface: (a) pseudo-4-fold hollow site; (b) 4-fold bridging site.

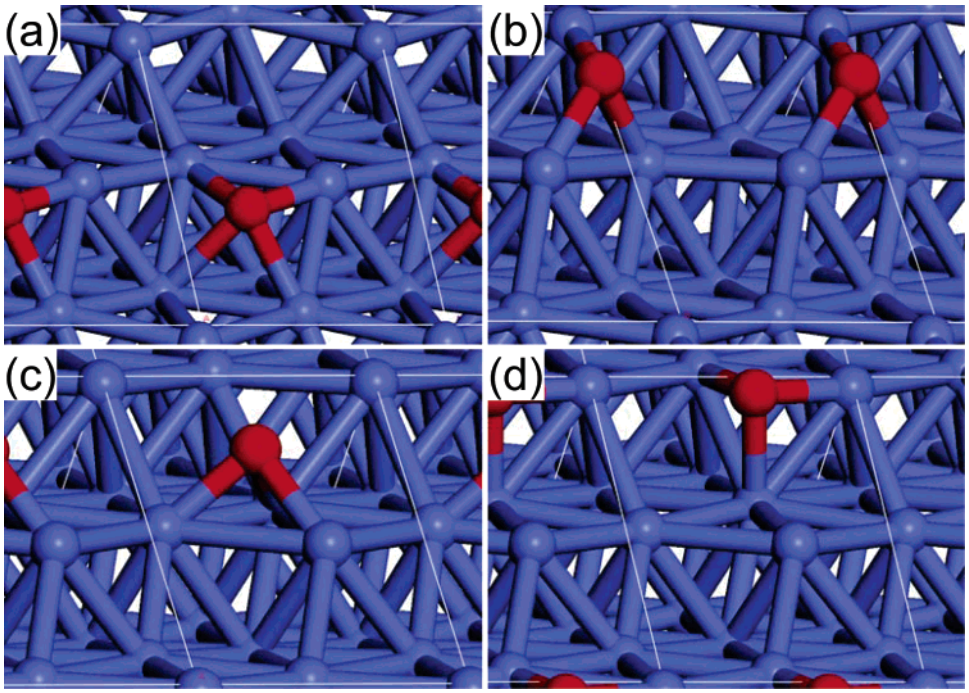

Figure 12. Perspective views of O adatoms adsorbed in four different sites on the Co{11$\bar{2}$4} surface: (a) pseudo-4-fold site; (b) asymmetrical 3-fold site; (c) 3-fold site on terrace; (d) 3-fold site on step.

the reaction barriers agree to within 5 kJ/mol. Two initial states of chemisorbed CO and the corresponding transition states calculated with the (2 × 1) surface unit cells are shown in Figure 13. The pathway shown in (a) and (b) starts with CO bound to the 4-fold site. At the transition state, the C adatom relaxes inward in the 4-fold site and O starts to form bridging bonds to the Co atoms on the step edge. The C−O distance at the transition state is 1.94 Å. The barrier corresponding to this transition state is 89 kJ/mol with respect to the initial chemisorbed CO. The transition state is 48.5 kJ/mol lower than the energy for gas-phase CO which suggests the direct dissociation of CO from the gas phase over the surface if the reaction is carried out at low surface coverage. An alternative pathway shown in (c) and (d) starts from CO chemisorbed in the 3-fold site on the terrace. The transition state corresponds to C occupying the same 3-fold hollow site and O forming bridging bonds to the Co atoms on the upper edge. The C−O distance at this transition state is 2.05 Å. The activation barrier along this path is 136 kJ/mol with respect to the initial state, which is higher than that found for the previous path. In addition, the barrier for this path is ∼5 kJ/mol higher in energy than the energy for gas-phase CO. Both transition states lead to the same final states where the C adatom occupies the pseudo-4-fold site (Figure 11a) and the O adatom sits in asymmetrical 3-fold site (Figure 12b). The overall reaction energy is −42 kJ/mol. This is similar for both pathways as the CO adsorption energies in their initial states are similar.

3.2.4. General Discussion. The most stable adsorption energies for CO, C, and O on each of the surfaces at the corresponding adsorption sites are collected together for comparison in Table 5. On the basis of these adsorption energies and calculated C−O bond strength, the overall reaction energies with respect to molecular CO, $\Delta E_{rxn,CO}$, for CO dissociation on these surfaces were subsequently calculated and included in the table. The effective reaction barriers ($\Delta E_{act,CO}$), i.e., the total energy difference between the transition state and sum of the clean slab and isolated CO molecule in the gas phase, over these surfaces is also listed in Table 5. In cases where multiple reaction paths were examined, we show only the lowest energy transition state. According to these results, the change in the adsorption energies for CO on different surfaces is very small. While there are significant differences in the O adsorption energies (∼ 50 kJ/mol), the change in C adsorption energies is even greater, ∼100 kJ/mol. As the result of the strong C−Co and O−Co chemisorption bond, the dissociation of CO is exothermic on all four surfaces. The stronger C−Co and O−Co bonds on the stepped {10$\bar{1}$2} and {11$\bar{2}$4} surfaces make the overall dissociation of CO on the surface even more exothermic.

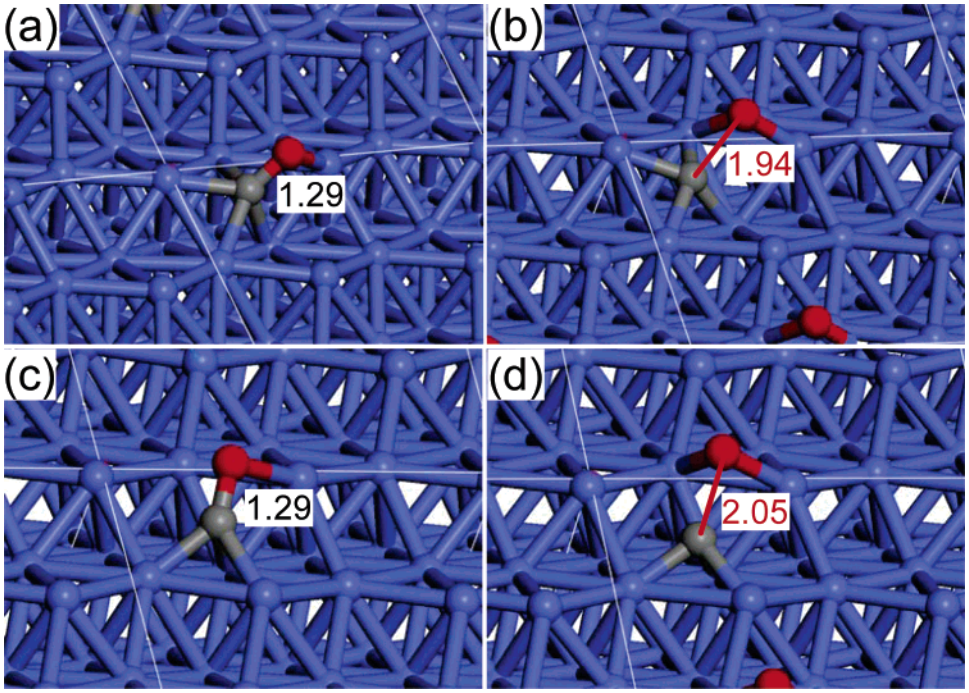

Figure 13. Two initial structures, (a) and (c), and their corresponding transition state structures, (b) and (d), for CO dissociation at the step edge of the Co{11$\bar{2}$4} surface: (a) chemisorbed CO in pseudo-4-fold hollow site; (b) four-fold site−bridge site transition state; (c) chemisorbed CO in pseudo-3-fold site; (d) three-fold site−bridge site transition state.

TABLE 5: DFT Calculated Energies for CO Adsorption and Dissociation on Different Co Surfaces, in kJ/mol[a]

	{0001}	{11$\bar{2}$0}	{10$\bar{1}$2}	{11$\bar{2}$4}
$\Delta E_{ads,CO}$	−160.4	−159.6	−164.6	−164.4
$\Delta E_{ads,C}$	−660.8	−684.4	−753.8	−716.6
$\Delta E_{ads,O}$	−544.0	−524.5	−576.9	−558.9
$\Delta E_{rxn,CO}$	−100.3	−104.4	−226.2	−171.0
$\Delta E_{act,CO}$	72.5	40.0	−28.7	−48.5

[a] The calculated CO bond strength, D_{CO} = 1104.5 kJ/mol, was used in calculating overall reaction energies.

The C−O distance at all of the transition states is significantly elongated as compared with the gas-phase CO bond length. The increased C−O distance at the transition states indicates that the barrier for CO dissociation is located at the exit channel, i.e., a "late transition state". The late transition state has been well-documented for CO dissociation on many transition metal surfaces, including Co.[44,46,51−53] Late transition states typically have structural and bonding properties resembling that of their product states which has been demonstrated previously for NO dissociation on Pt surfaces.[32] There is generally a linear relationship between the activation energy and stability of the product state for a reaction with a late transition state such as CO dissociation.[51] At first sight, this principle does not appear to hold for CO dissociation over Co{10$\bar{1}$2} and {11$\bar{2}$4}. A closer examination of the results reveals that both the C and O adatoms take on unique stable adsorption sites in the product state whereby they are stabilized by structural changes that take place at the step edge. The product state is much more stabilized than that which might be expected by relating it to other surfaces. The structural changes, however, have not yet formed in the transition state, so the transition state is in a much less stabilized configuration. In the reaction over Co{10$\bar{1}$2}, for example, the most stable 4-fold adsorption sites for C and O adatoms were not accessible through either of the transition states shown in parts a and b of Figure 9. The immediate product state just prior to the reconstruction has an overall reaction energy, $\Delta E_{rxn,CO}$, of −159.4 kJ/mol, with respect to the gas phase CO. If we approximate this energy as the product state energy, the activation barriers can be correlated linearly with the overall reaction energies as that is shown in Figure 14.

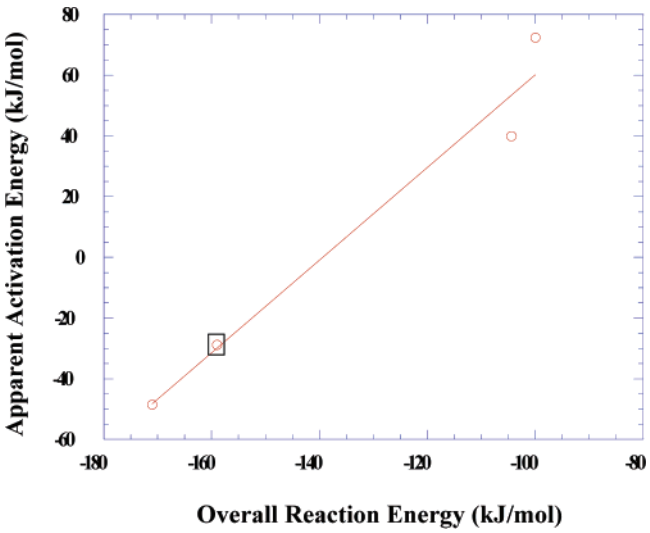

Figure 14. Linear correlation between the DFT calculated apparent activation energies and the overall reaction energies for CO activation over the Co surfaces. The point depicted at ΔE_{rxn} = −159 kJ/mol for Co{10$\bar{1}$2}, however, is not the stable product state. The stable product state on Co{10$\bar{1}$2} corresponds to an overall heat of reaction of −226.2 kJ/mol which breaks down the linear correlation.

These results also indicate that care must be taken when general principles such as linear free energy relationships are applied to specific reaction systems, as we demonstrated previously for the d-band center model.[54] For CO dissociation on the stepped surfaces, major factors contributing to the change of the dissociation barrier with respect to the close-packed surface include the added stabilization of the product state, i.e., O and C adatoms, provided by the steps. The dissociation of CO is accompanied by significant surface reconstruction which

modifies the reaction coordinate. One of the basic assumptions in deriving the linear free energy relationship is that the reactions follow a common pathway. The change in the reaction coordinate which occurs here due to reconstruction departs from the assumption of a common path.

The effective barriers for CO dissociation are positive on Co-{0001} and {11$\bar{2}$0} but negative on {10$\bar{1}$2} and {11$\bar{2}$4}. A negative effective activation barrier indicates that the total energy of the transition state is lower than that of the gas-phase CO molecule approaching the surface. Therefore, channels for direct CO dissociation may exist on the stepped {10$\bar{1}$2} and {11$\bar{2}$4} surfaces. This is consistent with the experimentally observed dissociation of CO on {10$\bar{1}$2} at relatively low temperature.[19,24]

IV. Conclusions

First principles density functional theory was used to analyze the first steps in the mechanism for Fischer−Tropsch synthesis, i.e., CO adsorption and activation over close-packed {0001}, corrugated {11$\bar{2}$0}, and stepped {10$\bar{1}$2} and {11$\bar{2}$4} surfaces. The calculated structure and energies for CO adsorption are in good agreement with experimental reported results. The adsorption of CO was calculated to be exothermic, only varying to within a very small range between −160.4 and −164.6 kJ/mol on all the surfaces examined. The surface structure does not appear to appreciably affect the CO adsorption energy. Stepped surfaces, however, do provide more types of sites for CO adsorption and in addition lead to more metastable adsorption configurations. High-coordinated adsorption sites resulted in longer C−O bonds in chemisorbed CO but the Co−CO chemisorption bond remained nearly the same. The adsorption energy of CO tends to increase as the CO coverage is reduced. This increase levels off, however, at much lower coverages whereby the lateral interactions become much smaller.

The dissociation of CO on all these surfaces proceeds through a late transition state which has a pronounced C−O stretch with C−O distances that are between 1.8 and 2.2 Å. The coverage of adsorbates can be used to modulate CO dissociation by blocking adsorption sites for product C and O adatoms. On all of the surfaces considered in the present study, the dissociation of CO is exothermic with respect to gas-phase CO. Lower surface coverages lead to the more favorable energetics. If chemisorbed CO is used as reference state, the reaction on Co-{0001} and {11$\bar{2}$0} becomes endothermic while remaining exothermic on Co{10$\bar{1}$2} and {11$\bar{2}$4}. The activation barrier for CO dissociation is sensitive to the surface structure. More open and stepped surfaces which provide strong binding sites for C and O adatoms are favorable for CO dissociation. On Co{10$\bar{1}$2} and {11$\bar{2}$4}, pathways which have activation energies that lie below the gas-phase CO at low coverages were identified. The existence of these low energy pathways on the stepped surfaces allows a CO molecule from the gas phase to dissociate spontaneously. This is consistent with the observed high reactivity of the stepped surface toward CO dissociation. While the overall product energies in general follow the activation energies, a linear relationship breaks down as the result of changes in the reaction coordinate due to the reconstruction at the steps of the Co{10$\bar{1}$2} surface that occurs after the formation of the transition state.

Acknowledgment. Funding of the project from National Energy Technology Laboratory of US Department of Energy (Grant No. DE-FG26-01NT41275) as well as the computer time allocated at the Pittsburgh Supercomputing Center on the Terascale Supercomputer (Grant No. ENG010004P) are greatly acknowledged. We also thank Dr. A. Cugini and D. Sorescu from DOE-NETL for helpful discussions.

References and Notes

(1) Anderson, R. B. *The Fischer−Tropsch Synthesis*; Academic Press: New York, 1984.
(2) Vannice, M. A. Catalytic Activation of Carbon Monoxide on Metal Surfaces. In *Catalysis*: *Science and Technology*; Anderson, J. R., Boudart, M., Eds.; Springer-Verlag: Berlin, 1982; Vol. 3; p 139.
(3) Horn, K.; Bradshaw, A.; Jacobi, K. *Surf. Sci.* **1978**, *72*, 719.
(4) Iglesia, E.; Reyes, S. C.; Madon, R. J.; Soled, S. L. Selectivity Control and Catalyst Design in the Fischer−Tropsch Synthesis−Sites, Pellets, and Reactors. In *Advances in Catalysis*; Academics Press: New York, 1993; Vol. 39; p 221.
(5) Iglesia, E. *Appl. Catal., A* **1997**, *161*, 59.
(6) Van der Laan, G. P.; Beenackers, A. *Catal. Rev.-Sci. Eng.* **1999**, *41*, 255.
(7) Geerlings, J. J. C.; Wilson, J. H.; Kramer, G. J.; Kuipers, H.; Hoek, A.; Huisman, H. M. *Appl. Catal., A* **1999**, *186*, 27.
(8) Ciobica, I. M.; Kramer, G. J.; Ge, Q.; Neurock, M.; van Santen, R. A. *J. Catal.* **2002**, *212*, 136.
(9) Bridge, M. E.; Comerie, C. M.; Lambert, R. M. *Surf. Sci.* **1977**, *67*, 393.
(10) Lahtinen, J.; Vaari, J.; Kauraala, K. *Surf. Sci.* **1998**, *418*, 502.
(11) Papp, H. *Surf. Sci.* **1983**, *129*, 205.
(12) Lahtinen, J.; Vaari, J.; Kauraala, K.; Soares, E. A.; Van Hove, M. A. *Surf. Sci.* **2000**, *448*, 269.
(13) Greuter, F.; Heskett, D.; Plummer, E. W.; Freund, H. J. *Phys. Rev. B* **1983**, *27*, 7117.
(14) Papp, H. *Surf. Sci.* **1985**, *149*, 460.
(15) Toomes, R. L.; King, D. A. *Surf. Sci.* **1996**, *349*, 1.
(16) Gu, J.; Yeo, Y. Y.; Sim, W. S.; King, D. A. *J. Phys. Chem. B* **2000**, *104*, 4684.
(17) Jenkins, S. J.; King, D. A. *J. Am. Chem. Soc.* **2000**, *122*, 10610.
(18) Welz, M.; Moritz, W.; Wolf, D. *Surf. Sci.* **1983**, *125*, 473.
(19) Prior, K. A.; Schwaha, K.; Lambert, R. M. *Surf. Sci.* **1978**, *77*, 193.
(20) Venvik, H. J.; Borg, A.; Berg, C. *Surf. Sci.* **1998**, *397*, 322.
(21) Venvik, H. J.; Berg, C.; Borg, A. *Surf. Sci.* **1998**, *402−404*, 57.
(22) Bardi, U.; Rovida, G. In *Studies in Surafce Science and Catalysis*; Morterra, C., Zecchina, A., Costa, G., Eds.; Elsevier: Amsterdam, 1989; Vol. 48, p 49.
(23) Geerlings, J. J. C.; Zonnevylle, M. C.; de Groot, C. P. M. *Surf. Sci.* **1991**, *241*, 302.
(24) Geerlings, J. J. C.; Zonnevylle, M. C.; de Groot, C. P. M. *Surf. Sci.* **1991**, *241*, 315.
(25) Kresse, G.; Hafner, J. *Phys. Rev. B* **1993**, *48*, 13115.
(26) Kresse, G.; Hafner, J. *Phys. Rev. B* **1993**, *47*, 558.
(27) Kresse, G.; Furthmuller, J. *Comput. Mater. Sci.* **1996**, *6*, 15.
(28) Vanderbilt, D. *Phys. Rev. B* **1990**, *41*, 7892.
(29) Lide, D. R. *CRC Handbook of Chemistry and Physics*; CRC Press: Boca Raton, 2004; Vol. 84.
(30) Perdew, J. P.; Chevary, J. A.; Vosko, S. H.; Jackson, K. A.; Pederson, M. R.; Singh, D. J.; Fiolhais, C. *Phys. Rev. B* **1992**, *46*, 6671.
(31) Monkhorst, H. J.; Pack, J. D. *Phys. Rev. B* **1976**, *13*, 5188.
(32) Ge, Q.; Neurock, M. *J. Am. Chem. Soc.* **2004**, *126*, 1551.
(33) Ge, Q.; Neurock, M.; Wright, H. A.; Srinivasan, N. *J. Phys. Chem. B* **2002**, *106*, 2826.
(34) Ge, Q.; Kose, R.; King, D. A. Adsorption energetics and bonding from femtomole calorimetry and from first principles theory. In *Advances in Catalysis*; Gates, B. C., Knozinger, H., Eds.; Academic Press, Inc.: San Diego, CA, 2000; Vol. 45; p 207.
(35) Neurock, M. *J. Catal.* **2003**, *216*, 73.
(36) Mills, G.; Jonsson, H.; Schenter, G. K. *Surf. Sci.* **1995**, *324*, 305.
(37) Henkelman, G.; Uberuaga, B. P.; Jonsson, H. *J. Chem. Phys.* **2000**, *113*, 9901.
(38) Henkelman, G.; Jonsson, H. *J. Chem. Phys.* **2000**, *113*, 9978.
(39) Kresse, G.; Furthmuller, J. VASP, the Guide, 2005.
(40) Sheppard, N.; Nguyen, T. T. The vibrational spectra of carbon monoxide chemsirobed on the surfaces of metal catalysts−A suggested scheme of interpretation. In *Advances in Infrared and Raman Spectroscopy*; Clark, R. J. H., Hester, R. E., Eds.; Heyden: London, 1978; Vol. 5, p 67.
(41) Ziegler, T. *Chem. Rev.* **1991**, *91*, 651.
(42) Van Santen, R. A.; Neurock, M. *Catal. Rev.-Sci. Eng.* **1995**, *37*, 557.
(43) Mortensen, J. J.; Kaasbjerg, K.; Frederiksen, S. L.; Norskov, J. K.; Sethna, J. P.; Jacobsen, K. W. *Phys. Rev. Lett* **2005**, *95*, 216401.
(44) Morikawa, Y.; Mortensen, J. J.; Hammer, B.; Norskov, J. K. *Surf. Sci.* **1997**, *386*, 67.
(45) Mavrikakis, M.; Baumer, M.; Freund, H. J.; Norskov, J. K. *Catal. Lett.* **2002**, *81*, 153.

(46) Ciobica, I. M.; van Santen, R. A. *J. Phys. Chem. B* **2003**, *107*, 3808.
(47) Gong, X. Q.; Raval, R.; Hu, P. *Surf. Sci.* **2004**, *562*, 247.
(48) Somorjai, G. A. *Introduction To Surface Chemistry and Catalysis*; Wiley: New York, 1994.
(49) Masel, R. I. *Principles of Adsorption and Reaction on Solid Surfaces*; Wiley: New York, 1996.
(50) Ge, Q.; Jenkins, S. J.; King, D. A. *Chem. Phys. Lett.* **2000**, *327*, 125.
(51) Liu, Z. P.; Hu, P. *J. Chem. Phys.* **2001**, *114*, 8244.
(52) Liu, Z. P.; Hu, P. *J. Am. Chem. Soc.* **2003**, *125*, 1958.
(53) Li, T.; Bhatia, B.; Sholl, D. S. *J. Chem. Phys.* **2004**, *121*, 10241.
(54) Ge, Q.; Neurock, M. *Chem. Phys. Lett.* **2002**, *358*, 377.